Available Online

J. Sci. Res. **15** (2), 383-399 (2023)

JOURNAL OF SCIENTIFIC RESEARCH

www.banglajol.info/index.php/JSR

Simulation of Nanofluid Flow in Porous Square-Shaped Enclosures

M. J. H. Munshi[1*], M. S. Islam[2], M. R. R. Khandaker[3], M. S. Hossain[4]

[1]Department of Mathematics, Hamdard University Bangladesh (HUB), Hamdard Nagar, Gazaria, Munshigonj-1510, Bangladesh

[2]Department of Mathematics, Sonargaon University (SU), Green Road, Tajgaon, Dhaka-1215, Bangladesh

[3]Department of Mathematics, Dhaka Imperial College, Aftab Nagar, Dhaka-1212, Bangladesh

[4]Department of Arts and Sciences, Ahsanullah University of Science and Technology (AUST), Love Road, Tejgaon Industrial Area, Dhaka-1208, Bangladesh

Received 10 September 2022, accepted in final revised form 1 February 2023

Abstract

Augmentation of heat transfer can be in so many ways, heat transfer of a nanofluid in a porous is one of the most recent methodologies. In this analysis, the physical properties of water as the base fluid and copper as the nanoparticles exercise. The Finite element method is applied to obtain numerical solutions. The effects of the Darcy number, Richardson number and solid volume fraction of nanofluids on the streamlines, isotherms, dimensionless temperature, velocity profiles, and average Nusselt numbers and average fluid temperature examined graphically. It has found that both the Richardson number and solid volume fraction have a noteworthy influence on streamlines and isotherms. Darcy number has a good control parameter for heat transfer in fluid flow through a porous medium in the enclosure. A heat transfer correlation of the average Nusselt number for various Darcy numbers and solid volume fraction presented here. Finally, for the validation of the existing work, the current results are compared with the published results, and a favorable agreement attained. Besides this, heat transfer in the square enclosure remains better than for the other enclosures with the wavy walls or curved walls.

Keywords: Nanofluid; Porous medium; Constant heat flux; Finite element method; Lid-driven.

doi: http://dx.doi.org/10.3329/jsr.v15i2.61667 J. Sci. Res. **15** (2), 383-399 (2023)

1. Introduction

Heat is the form of energy that can be transferred from one system to another as a result of temperature differences. The science that deals with the determination of the rates of such energy transfers are heat transfer. Heat transfer in an enclosure is an important development and an area of very rapid growth in the contemporary trend of heat transfer research. Analysis of natural convection heat transfer and fluid flow in enclosures has been extensively made using numerical techniques experiments because of its wide

* *Corresponding author*: jahir.buet.bd@gmail.com

applications and interest in engineerings such as nuclear energy, double pane windows, heating and cooling of buildings, solar collectors, electronic cooling, micro-electromechanical systems (MEMS). Nanofluid is a composite fluid that consists of nanoparticles with a dimension measured in nanometers, less than 100 nm, dispersed in a based fluid. Over the past decade, many researchers reported that nanofluids possess substantially higher thermal conductivity [1-4]. The numerical study has been performed by Rahman *et al*. [5] using unsteady natural convection in Al_2O_3-water nano liquid filled in an isosceles triangular enclosure with sinusoidal thermal boundary condition on the bottom wall introducing nanofluid in it. Chamkha *et al.* [6] worked on mixed convection flow in single- and double-lid driven square cavities filled with water- Al_2O_3 nanofluid: Effect of viscosity models. The most usage of the mixed convection flow with lid-driven effect is to include the cooling of electronic devices, lubrication technologies, drying technologies, etc. Mansour *et al.* [7] have examined the numerical simulation of mixed convection flows in a square lid-driven cavity partially heated from below using nanofluid. Ahmed *et al*. [8] have analyses of mixed convection from a discrete heat source in enclosures with two adjacent moving walls filled with micropolar nanofluids. Moreover, Parvin *et al.* [9] have studied the Flow and Heat Transfer Characteristics for MHD Free Convection experimentally in an Enclosure with a Heated Obstacle. Therefore, Billah *et al*. [10] studied the numerical simulation of Heat Transfer Enhancement of Copper-water Nanofluids in an Inclined Lid-driven Triangular Enclosure. Abu-Nada *et al*. [11] investigated the effects of inclination angle on natural convection in enclosures filled with Cu-water nanofluid. Oztop *et al.* [12] analyzed the numerical study of natural convection in partially heated rectangular enclosures filled with nanofluid. Bensouici *et al*. [13] numerically investigate mixed convection of nanofluids inside a lid-driven cavity heated by a central square heat source. Guo *et al*. [14] studied mixed convection in rectangular cavities at various aspect ratios with moving isothermal sidewalls and a constant flux heat source on the bottom wall. Parvin and Nasrin [17] conducted the effects of Reynolds and Prandtl numbers on mixed convection in an octagonal channel with a heat-generating hollow cylinder. Later, Munshi *et al.* [18] extended their works by considering a mixed convection double lid-driven square cavity with an inside elliptic heated block. At the same time, a numerical study of mixed convection in square lid-driven with an internal elliptic body and constant flux heat source on the bottom wall was presented by Munshi *et al*. [19].

To the author's knowledge, the problem simulation of nanofluid in a porous square-shaped enclosure has not been treated so far. The present study addresses the effects of the Darcy number, solid volume fraction, and Richardson number on such geometry's thermal and flow fields.

The rest of the paper is compiled as follows. Sections 2 and 3 formally approves the mathematical formula for this work. Section 4 describes the simulation for validation of this work. A thorough discussion of simulation results takes place in Section 5. Finally, conclusions and some future developments are set out in Section 6.

2. Physical Model

Consider the physical model consisting of a porous square shape enclosure with sides of length L, within which a heated elliptic obstacle is placed at a different location. In the square-shaped enclosure, the left and right walls are kept to be cooled.

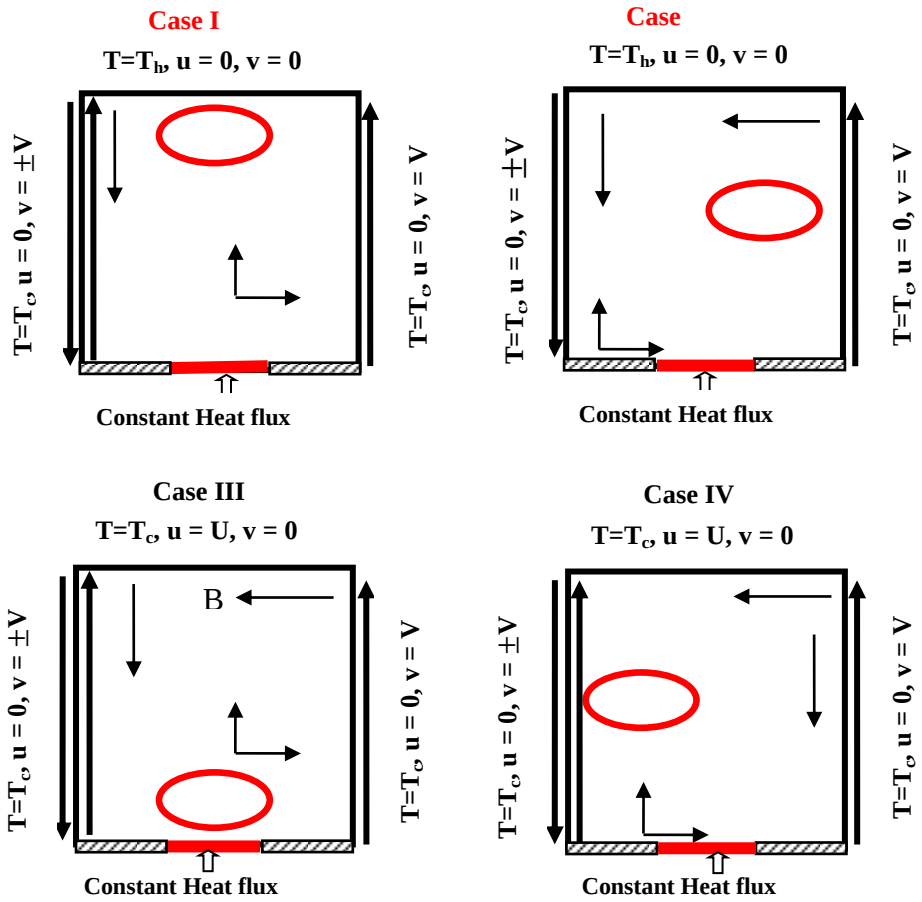

Fig. 1. Schematic diagram with boundary condition of the present problem.

A constant flux heat source is located on the part of the bottom wall, and the other parts are thermally insulated. The top wall and elliptic obstacle heated the temperature. The right wall moves upwards while the left wall moves upwards and downwards with uniform velocity $\pm V$. The base fluid water and nanoparticles of copper are in thermal equilibrium.

3. Mathematical Formulation

The mass, momentum, energy, and volume fraction equations for the laminar and steady-state two-dimensional incompressible flow solution are as follows:

$$\underline{\nabla}.\underline{q} = 0$$

$$\rho_{nf}\left(\underline{q}.\underline{\nabla}u\right) = -\frac{\partial p}{\partial x} + \mu_{nf}\nabla^2 u - \frac{(\rho\beta)_{nf}}{k}\nu u$$

$$\rho_{nf}\left(\underline{q}.\underline{\nabla}v\right) = -\frac{\partial p}{\partial y} + \mu_{nf}\nabla^2 v - \frac{(\rho\beta)_{nf}}{k}\nu v + (\rho\beta)_{nf} g\beta(T - T_c) - \sigma_{nf}B_0^2 v$$

$$\underline{q}.\underline{\nabla}T = \alpha_{nf}\nabla^2 T$$

where u, v are the velocity components in the x and y directions, ρ is the density, p is the pressure, ν is the kinematic viscosity, g is the acceleration due to gravity, α is the thermal diffusivity, β is the volume expansion coefficient, T is the temperature.

The boundary conditions for the present problem are specified as follows:

On top wall: $T = T_h$, $u = 0$, $v = 0$

On cold right wall with moving: $T = T_c$, $u = 0$, $v = V$

On cold left wall with moving: $T = T_c$, $u = 0$, $v = \pm V$

On bottom wall: $\dfrac{\partial T}{\partial y} = \begin{cases} 0, & for\ 0 < X < (1-\varepsilon)/2 \\ -u & for\ (1-\varepsilon)/2 \times (1+\varepsilon)/2 \\ 0 & for\ (1+\varepsilon)/2 < X < 1 \end{cases}$

The effective density and thermal diffusivity of the nanofluid are:

$$\rho_{nf} = (1-\varphi)\rho_f + \varphi\rho_s$$

$$\alpha_{nf} = \frac{\mathrm{k}_{nf}}{(\rho c_p)_{nf}}$$

The heat capacity and thermal expansion coefficient of the nanofluid are:

$$(\rho c_p)_{nf} = (1-\varphi)(\rho c_p)_f + \varphi(\rho c_p)_s$$

$$(\rho\beta)_{nf} = (1-\varphi)(\rho\beta)_f + \varphi(\rho\beta)_s$$

Brinkman [Brinkman (15)] as follows:

$$\mu_{nf} = \frac{\mu_f}{(1-\varphi)^{2.5}}$$

The effective thermal conductivity of nanofluid is as follows (by the Maxwell model [16]):

$$k_{nf} = \frac{k_s + 2k_f - 2\varphi(k_f - k_s)}{k_s + 2k_f + \varphi(k_f - k_s)} \times k_f$$

Table 1. Thermo-physical properties of water-Copper nanofluid [8].

Physical properties	Water	Copper
C_p	4179	385
ρ	997.1	8933
k	0.613	401
β	21×10^{-5}	1.67×10^{-5}

Dimensional variables used for making the governing equations (1) - (5) into dimensionless form are stated as follows:

$$X = \frac{x}{L}, Y = \frac{y}{L}, U = \frac{u}{U_0 \alpha_f}, V = \frac{v}{U_0 \alpha_f}, P = \frac{p}{\rho_{nf} U_0^2}, \theta = \frac{T - T_c}{T_h - T_c},$$

$$Pr = \frac{\upsilon_f}{\alpha_f}, Da = \frac{K}{L^2}, Re = \frac{U_0 L}{\upsilon_f}, Gr = \frac{g\beta(T_h - T_C)L^3}{{\nu_f}^2} \text{ and } Ri = \frac{Gr}{RE^2}.$$

After the substitution of the dimensional variables into the equations (1) - (5), we get the following dimensionless equations as

$$\frac{\partial U}{\partial X} + \frac{\partial V}{\partial Y} = 0$$

$$U\frac{\partial U}{\partial X} + V\frac{\partial U}{\partial Y} = -\frac{\partial P}{\partial X} + \frac{1}{Re}\frac{\mu_{nf}}{\rho_{nf}\gamma_f}\frac{1}{(1-\varphi)^{2.5}}\nabla^2 U - \frac{(\rho\beta)_{nf}}{\rho_{nf}\beta_f}\frac{1}{ReDa}U$$

$$U\frac{\partial V}{\partial X} + V\frac{\partial V}{\partial Y} = -\frac{\partial P}{\partial Y} + \frac{1}{Re}\frac{\mu_{nf}}{\rho_{nf}\gamma_f}\frac{1}{(1-\varphi)^{2.5}}\nabla^2 V - \frac{(\rho\beta)_{nf}}{\rho_{nf}\beta_f}\frac{1}{ReDa}V + \frac{(\rho\beta)_{nf}}{\rho_{nf}\beta_f}Ri\theta - \frac{Ha^2}{Re}V$$

$$U\frac{\partial \theta}{\partial X} + V\frac{\partial \theta}{\partial Y} = \frac{\alpha_{nf}}{\alpha_f}\frac{1}{RePr}\nabla^2\theta$$

The dimensionless boundary conditions would be adjusted as follows:

On the top wall: $\theta = 1, U = 0, V = 0$

On the right wall with moving: $\theta = 0, U = 0, V = 1$

On the cold left wall with moving: $\theta = 0, U = 0, V = \pm 1$

On the bottom wall: $\dfrac{\partial\theta}{\partial y} = \begin{cases} 0, \ for\ 0 < X < (1-\varepsilon)/2 \\ -1\ for(1-\varepsilon)/2 \times (1+\varepsilon)/2 \\ 0\ for(1+\varepsilon)/2 < X < 1 \end{cases}$

On the elliptic obstacle: $\theta = 1, U = 0, V = 0$

We define the local heat transfer coefficient $h_s = \frac{q^n}{[T_s - T_c]}$ at a given point on the heat source surface where $T_s(x)$ is the local temperature on the surface. Accordingly, the local Nusselt number and the average or over all Nusselt number can be obtained respectively as $N_u = \frac{h_x W}{k} = \frac{1}{\theta_s(X)}$ and $\overline{Nu} = \frac{\bar{h}W}{k} = \frac{1}{\varepsilon}\int_0^{\epsilon}\frac{1}{\theta_s(X)}dX$ where $\theta_s(X)$ is the local dimensionless temperature.

4. Numerical Implementation

The nonlinear governing partial differential equations, i.e., mass, momentum, and energy equations, are transferred into a system of integral equations by using the Galerkin weighted residual finite-element method. The integration involved in each term of these equations is performed with the aid Gauss quadrature method. The nonlinear algebraic equations so obtained are modified by the imposition of boundary conditions. These modified nonlinear equations are transferred into linear algebraic equations with the aid of Newton's method. Lastly, the Triangular Factorization method is applied to solve those linear equations.

4.1. *Validations*

The computer code and Guanghong *et al.* [14] were modified and used for the computations in the study. The working fluid is chosen Prandtl number Pr = 0.733. The left and right wall is kept heated $T_{h,}$ and the upper wall is kept at cold T_c. Performing simulation for natural convection in the lower wall is adiabatic. Streamlines and isotherms are plotted in Fig. 2. showing good agreement.

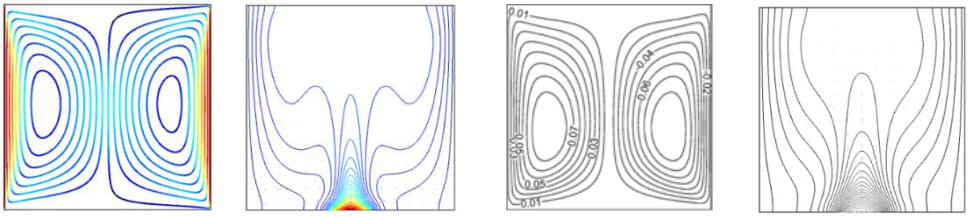

Fig. 2. (a) Present study (b) Guanghong *et al.* [14] obtained streamlines and isotherms for Re = 10, Gr = 10, Pr = 0.733, and Ri = 0.01.

4.2. *Grid independency study*

In order to determine the proper grid size for this study, a grid independence test is conducted with five types of mesh $Pr = 6.2, Gr = 10^4, Re = 100, Ri = 1$ and $\varphi = 2\%$. considering both the accuracy of numerical value, the present calculations are performed with 20438 nodes and 6686 elements grid system. This is described in Fig. 3.

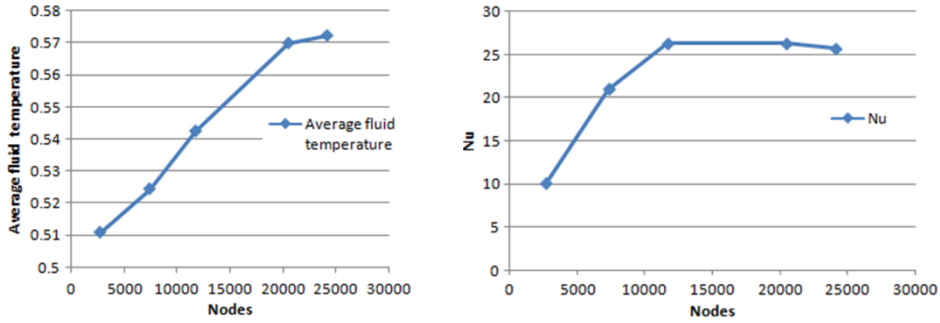

Fig. 3. Effects on (a) average fluid temperature and (b) average Nusselt number in the enclosure, while $\mathrm{Pr} = 6.2, \mathrm{Gr} = 10^4, \mathrm{Re} = 100, \mathrm{Ri} = 1$ and $\varphi = 2\%$.

Table 2. Grid sensitivity check at $\mathrm{Pr} = 6.2, \mathrm{Gr} = 10^4, \mathrm{Re} = 100, \mathrm{Ri} = 1$ and $\varphi = 2\%$.

Nodes	2646	7320	11670	20438	24087
Elements	862	1205	2233	6686	25918
Nu	9.99096	21.00239	26.28221	25.68892	27.47390
Temperature(θ_{ave})	0.51078	0.52438	0.54245	0.56993	0.57239

5. Results and Discussion

In this section, the results of the numerical study on mixed convection nanofluid flow in a lid-driven porous square enclosure with an eccentric elliptic body and constant flux heat source on the bottom wall are numerically presented. The results have been obtained for the Darcy number ranging from $1e^{-5}$ to $1e^{-2}$, Richardson number ranging from 0.01 to 10, solid volume fraction of nanoparticles ranging from 0 to 0.09, and the result are presented in distinct sections.

5.1. *Effect of darcy number (left wall lid moves downwards)*

The streamlines in the square enclosure for water-based copper nanofluid are shown in Fig. 4 for various cases of the moving lids, and when the Darcy number varies from $1e^{-5}$ to $1e^{-2}$ and at $Pr = 6.2, Gr = 10^4, Re = 100, Ri = 1$ and $\varphi = 2\%$. Fig. 4 shows the streamlines when the mixed convection effect is dominated for various moving lid orientations. For all cases, the moving lids have a stronger influence compared with the buoyancy force. It can be seen that when the right wall lid moves upwards and when the left wall lid moves downwards, two large separate vortices with perfectly symmetrical patterns about the square of the enclosure can be generated, which occupy most of the size of the enclosure. This is because the convection currents begin from the heated elliptic obstacle in a different location in the heated upper wall, and the left wall moves downward due to both buoyancy forces.

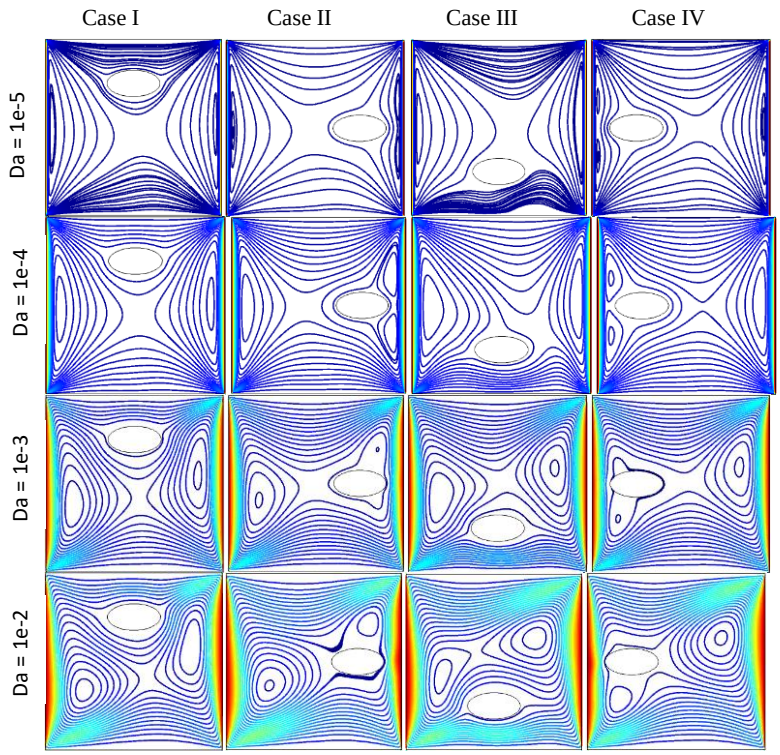

Fig. 4. Streamlines at different values of darcy number with left wall lid move downwards.

Isotherms for different values of Darcy numbers are presented in Fig. 5. With respect to isotherms; there is a clear accumulation of them adjacent to the constant flux heat source located at the bottom wall of the square enclosure. This is due to the strong temperature gradient in the horizontal direction which to the strong temperature gradient in the horizontal direction which gives an indication that the convection heat transfer because more significant compared to the conduction heat transfer. For all cases with increases in Darcy numbers, isotherms are concentrated near the right and bottom wall, and isotherms lines are more bending, which nears increasing heat transfer.

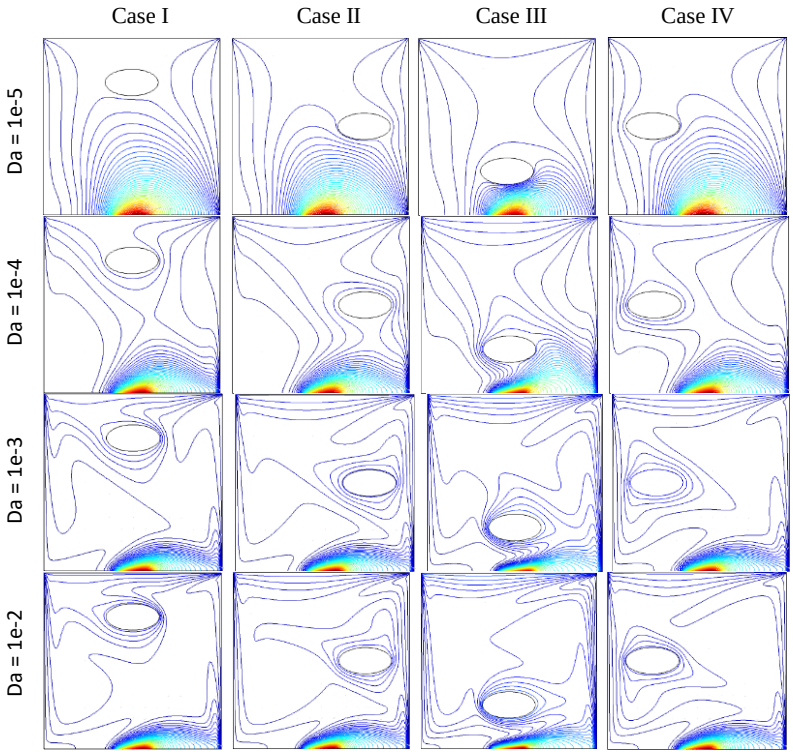

Fig. 5. Isotherms for different values of darcy number with left wall lid move downwards.

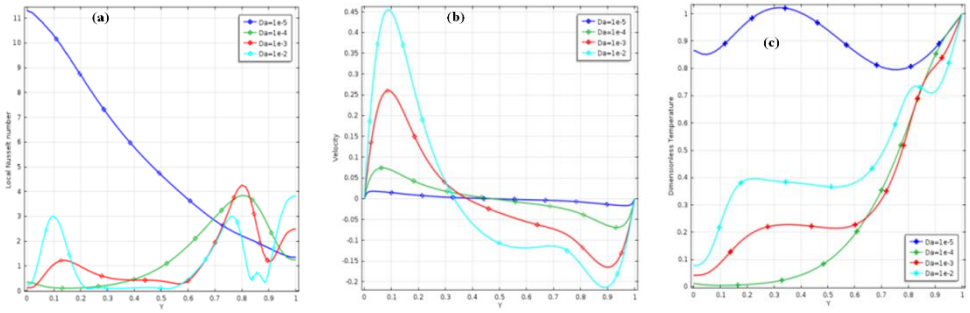

Fig. 6. Variation of (a) local Nusselt number, (b) velocity, and (c) dimensionless temperature along the right wall of the square enclosure with left wall lid move downwards in various Darcy numbers.

Variations of the local Nusselt number along the right wall are shown in Fig. 6(a). As can be observed from Fig., in the whole portion of the enclosure, the local Nusselt number decreases with an increase in the Darcy number. Variations of the velocity component along the right are shown in Fig. 6(b). It can be seen from the Fig. that the absolute value of the maximum and minimum value of velocity increases with increasing the Darcy number. Fig 6(c) presents the temperature profiles along the right wall for different Darcy

numbers. As seen from Fig., the temperature value is decreased from the increasing Darcy numbers.

5.2. *Effect of darcy number (left wall lid move upwards)*

Figs. 7 and 8 illustrate the streamlines and isotherms when the different Darcy numbers effects moving lid orientations. In this case, flow strength increases inside the enclosure, and the flow field behavior for all cases is approximately similar to the one presented in Fig. 7. The only difference between these cases is two or more circulating vortices inside the enclosure. This increase in the Darcy number reduces the influence of the moving lids and causes to increase in the circulation intensity. The maximum streamlines for these cases can be found in the Darcy number$Da = 1e^{-2}$. Regarding the isotherms, for all moving lid orientations, the distributions of the isotherms increase gradually right wall lid move upwards compared with the left wall lid moving upwards. This is because the intensity of circulation increases due to the increase in the effect of the vortices coming from the buoyancy force effect when the Darcy number is increasing.

The local Nusselt number along $Y-$axis of the enclosure with different values of Darcy numbers are shown in Fig. 9(a). As seen from this Fig., minimum and maximum shape curves are obtained here. The lower value of the Darcy number local Nusselt number is a more significant change, but the higher value of the Darcy number is a less significant number. The variation of the velocity profile along $Y-$axis for different Darcy numbers of the enclosure is shown in Fig. 9(b). Maximum and minimum shape curves are found, and a lower value of Darcy number symmetric$X-$axis, but a higher value of Darcy number maximum shape curves are found, and the absolute value of the velocity profile is increased from the increasing of Darcy numbers. Fig. 9(c) presents the variation of dimensionless temperature along the $Y-$axis for different Darcy numbers. For the lower Darcy, the number temperature value has a more significant change, but for the higher Darcy, the number temperature value has a less significant change.

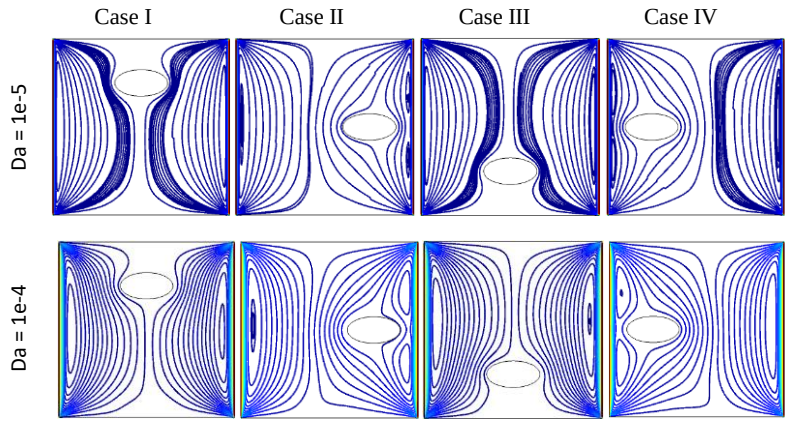

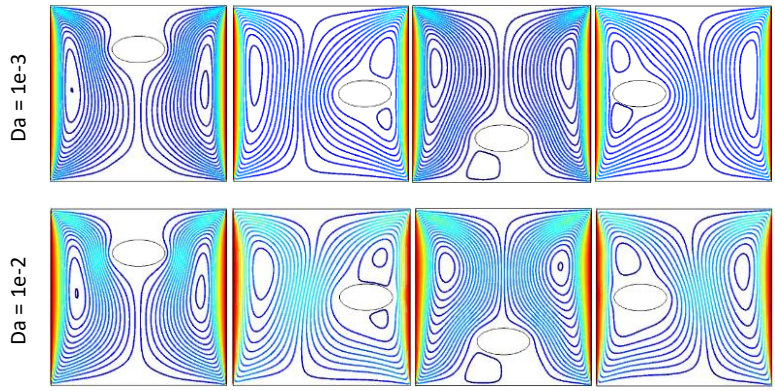

Fig. 7. Streamlines at different values of Darcy number with left wall lid move upwards.

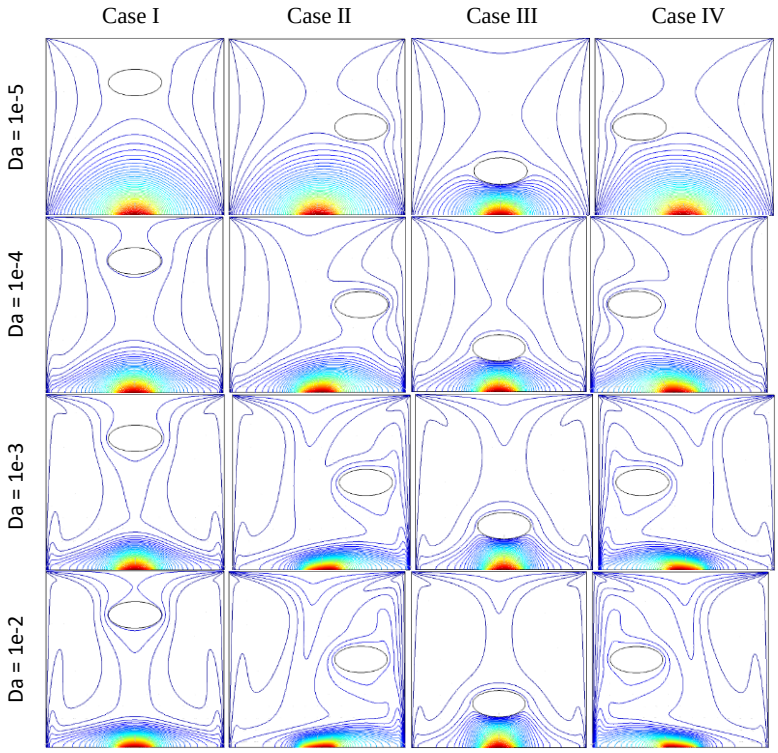

Fig. 8. Isotherms at different values of Darcy number with left wall lid move upwards.

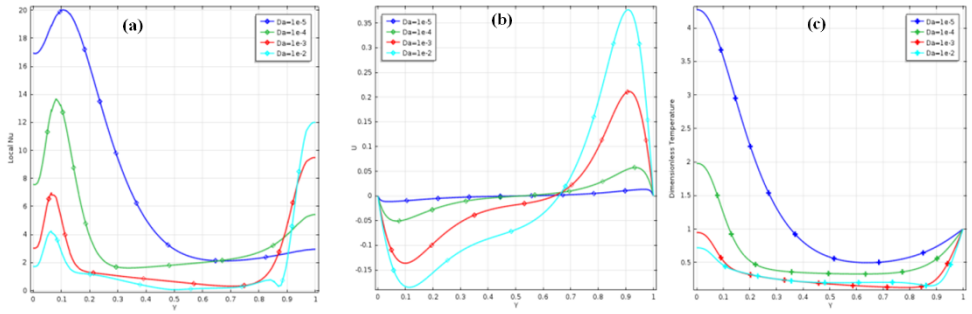

Fig. 9. Variation of (a) Local Nusselt number, (b) velocity, and (c) dimensionless temperature along the right wall of the square enclosure with left wall lid move upwards in various Darcy numbers.

5.3. *Effect of Richardson number (left wall lid move upwards)*

This section shows the mixed convection nanofluid flow resultsow in a lid-driven porous square enclosure with an eccentric elliptic body and constant flux heat source on the bottom wall filled with an electrically conductive fluid with $Pr = 6.2$ are presented. The results have been obtained for the Richardson number ranging from 0.01-10. The results are presented in terms of streamlines and isotherms inside the enclosure, the vertical velocity components, the local Nusselt number, and the dimensionless temperature of the heated wall.

Variation of streamlines and isotherms inside the enclosure with Richardson number is shown in Fig. 10, respectively. When the lower value of Richardson numbers, more fluid is raised inside the enclosure, and the moving lid becomes very strong. For the higher value of Richardson number, two cells are formed with two elliptic-shaped eyes lower side of the cavity, and also flow strength increases are shown in Fig. 10. Conduction dominant heat transfer is observed from the isotherms in Fig. 10. With the increase in Richardson number, isotherms concentrate near the bottom wall, and isotherms line are more bending which means increasing heat transfer through convection.

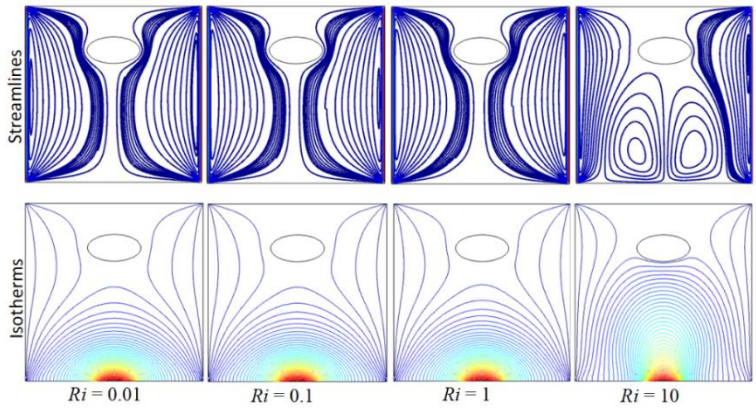

Fig. 10. Streamlines and isotherms at different values of Richardson number with left wall lid move upwards when $Da = 10^{-5}, Pr = 6.2, Ha = 25$ and $\phi = 2$ %.

The local Nusselt number along the bottom wall for different Richardson numbers with $Pr = 6.2, Ha = 25$ of the enclosure is shown in Fig. 11(a). Minimum and maximum shape curves are found, and $X < 0.3$ maximum shape curves are found, and $X > 0.3$ minimum shape curves are found, and the absolute value of the local Nusselt number (that is, heat transfer rate) is increased from the increasing of Richardson numbers.

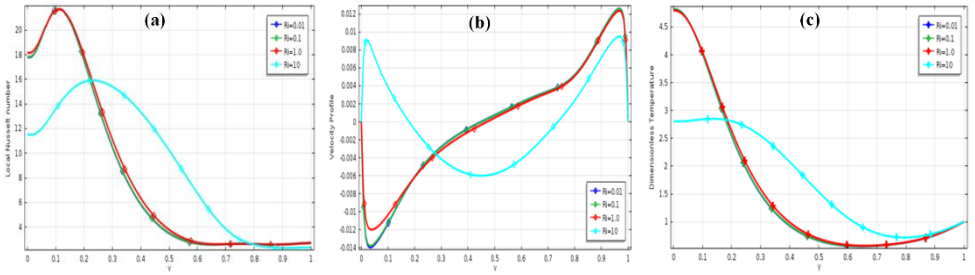

Fig. 11. Variation of (a) local Nusselt number, (b) velocity profile, and (c) dimensionless temperature along the right wall of the square enclosure with left wall lid move directions in various Richardson numbers upward when $Da = 10^{-5}, Pr = 6.2, Ha = 25$ and $\phi = 2$ %.

Variation of the vertical velocity component along the bottom wall for different Richardson numbers with $Pr = 6.2$ and $Ha = 25$ of the enclosure is shown in Fig. 11(b). It can be seen from Fig. that the absolute value of the maximum and minimum value velocity increases with increasing the Richardson number. For lower Richardson, the number value of velocity has a smaller change, but the higher Richardson number value of velocity has a larger change. Fig. 11 (c) presents the temperature profiles along the bottom wall for different Richardson numbers with $Pr = 6.2$ and $Ha = 25$. As seen from Fig., the temperature decreases from the increasing of Richardson numbers. For lower Richardson, the number temperature value has more significantly changed, but for higher Richardson, the number temperature value has less significance.

5.4. *Effect of solid volume fraction of nanoparticles (left wall lid move upward)*

Fig. 12 shows the effect of the solid volume fraction of nanoparticles with the left wall lid moving upward direction. The results are presented in terms of streamlines and isotherms inside the enclosure. For the lower values of volume fraction of nanoparticles flowing flow due to moving lid becomes very weak streamlines are little change, but for the higher volume fraction of nanoparticles, two cells are formed with two vortices on the lower side of the elliptic shape heated block and flow strength increases. Conduction dominant heat transfer is observed from the isotherms, as shown in Fig. 12. With the increase in the solid volume fraction of nanoparticles, isotherms concentrate near the bottom wall, and isotherms lines are more bending, which means increasing heat transfer through convection.

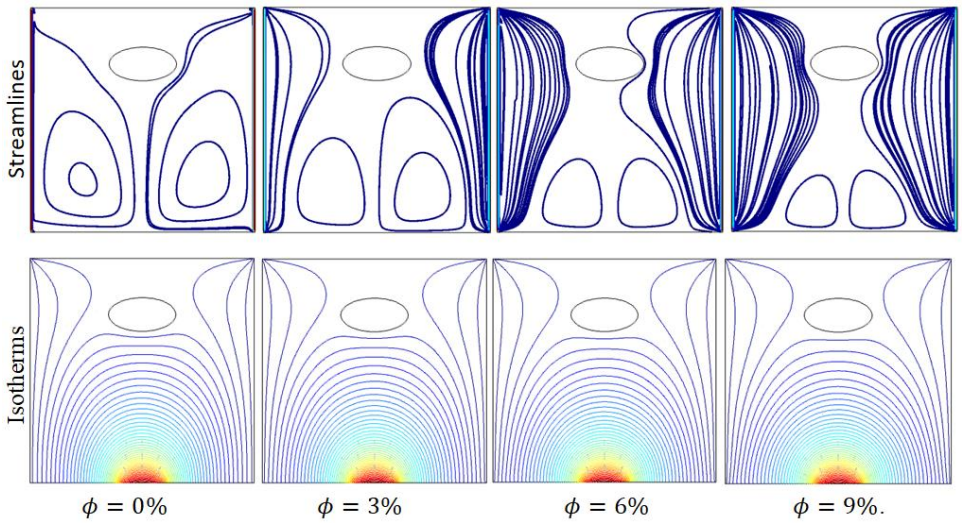

Fig. 12. Streamlines and isotherms at different values of solid volume fraction of nanoparticles with left lid move upward direction when $\phi = 0\ \%, 3\ \%, 6\ \%, 9\ \%$ when $Ri = 1, Da = 10^{-5}, Pr = 6.2$ and $Ha = 25$.

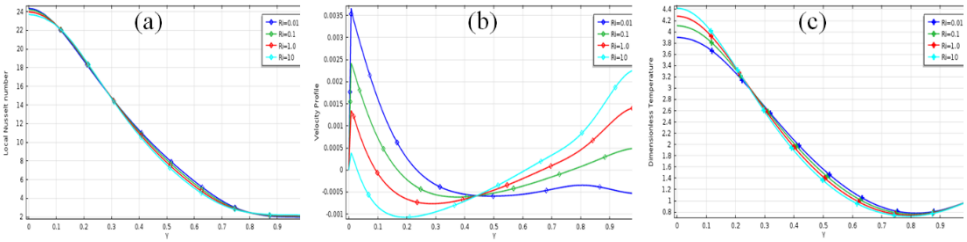

Fig. 13. Variation of (a) Local Nusselt number, (b) velocity profile, and (c) dimensionless temperature along the right wall of the square enclosure with left lid move upward direction in various solid volume fraction of nanoparticles when $Ri = 1, Da = 10^{-5}, Pr = 6.2$ and $Ha = 25$.

The local Nusselt number along the bottom wall for different values of volume fraction of nanoparticles with $Pr = 6.2, Ha = 25$ of the enclosure is shown in Fig. 13(a). Minimum and maximum shape curves are found, and the absolute value of the Local Nusselt number is decreased from the increasing volume fraction of nanoparticles. Variation of the vertical velocity component along the bottom wall for the different volume fractions of nanoparticles with $Pr = 6.2$ and $Ha = 25$ of the enclosure is shown in Fig. 13(b). It can be seen from the Fig. that the absolute value of the maximum and minimum value of velocity increases with increasing the volume fraction of nanoparticles. The lower volume fraction of nanoparticles' value of velocity has a smaller change, but the higher volume fraction of nanoparticles' value of velocity has a larger change. Fig. 13(c) presents the temperature profiles along the bottom wall for the different volume fractions of nanoparticles with $Pr = 6.2$ and $Ha = 25$. As seen from the Fig., the

temperature value is decreased from the increasing volume fraction of nanoparticles. For the lower volume fraction of nanoparticles, the temperature value has a more significantly changed, but for the higher volume fraction of nanoparticles, the temperature value has less significance.

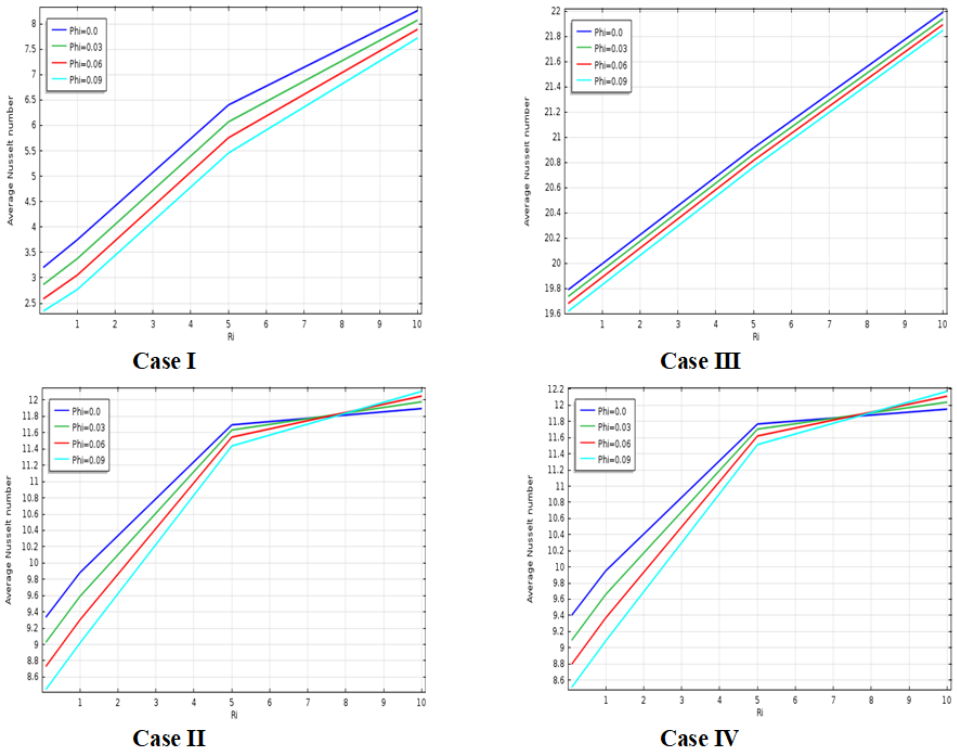

Fig. 14. Variation of average Nusselt number versus Richardson number for the different solid volume fractions of nanoparticles along the right wall where when $Da = 10^{-5}, Pr = 6.2$ and $Ha = 25$.

The influence of solid volume fraction of nanoparticles on average Nusselt number versus different Richardson numbers is displayed in Fig. 14 at when$Da = 10^{-5}, Pr = 6.2$ and $Ha = 25$. It is clearly observed that adding nanoparticles in the base fluid inside the porous enclosure causes an increase in the average Nusselt number. Also, the rate of increment on heat transfer clearly depends on the value of the Richardson number. It is also evident from this Figure that the value of the average Nusselt number grows as the percentage of nanoparticles increases from 0 to 9. This means that the addition of nanoparticles causes enhancement of the heat transfer for all considered values of the Richardson number.

6. Conclusion

A numerical study has been performed to investigate the effect of mixed convection nanofluid flow in a lid-driven porous square enclosure with **an** eccentric elliptic body and constant flux heat source on the bottom wall using the finite element method approach. Some important points can be drawn from the obtained results, such as

(a) Both Darcy and moving lid ordinations significantly affect the flow and thermal fields in the temperature.
(b) The type of nanofluid is a key factor for heat transfer enhancement. The highest values are obtained when using *Cu* nanoparticles.
(c) Fluids flow and heat transfer characteristics inside the cavity strongly depend upon the eccentric elliptic body. The average Nusselt number at the hot wall becomes higher, and the average fluid temperature in the cavity becomes lower for the lower values of the heater length as the considered Grashof number.
(d) Depending on the moving lid cases and Darcy number, different velocity profiles are observed.
(e) Richardson number is a good control parameter for heat transfer in fluid flow through a porous medium.
(f) The location of the heated block significantly affects the flow and thermal fields, together with the average Nusselt number result.
(g) The velocity of the fluid is augmented by the increase of the solid volume fraction of nanoparticles which results in an increase in heat transfer rate.
(h) Copper water nanofluid has greater merit in being used for heat transfer enhancement.

References

1. W. H. Azmi, K. V. Sharma, R. Mamat, and S. Anuar, J. Mechanic. Eng. Sci. **4**, 397 (2013). ttps://doi.org/10.15282/jmes.4.2013.4.0037
2. G. S. Rao, K. V. Sharma, S. P. Chary, R. A. Bakar, M. M. Rahman, K. Kadirgama, and M. M. Noor, J. Mechanic. Eng. Sci. **1**, 11 (2011).
3. L. S. Sundar and K. V. Sharma, J. Mechanic. Eng. Sci. **1**, 99 (2011). https://doi.org/10.15282/jmes.1.2011.9.0009
4. A. M. Hussein, R. A. Bakar, K. Kadirgama, and K. V. Sharma, Int. J. Automot. Mechanic. Eng. **7**, 850 (2013). https://doi.org/10.15282/ijame.7.2012.5.0070
5. M. M. Rahman, Hakan F. Oztop, S. Mekhilef, R. Saidur, and K. Al-Salem, Superlattices Microstruct. **67**, 181 (2014). https://doi.org/10.1016/j.spmi.2014.01.001
6. A. J. Chamkha and E. Abu-Nada, Euro. J. Mechanic B/Fluids **36**, 82 (2012). https://doi.org/10.1016/j.euromechflu.2012.03.005
7. M. A. Mansour, R. A. Mohamed, M. M. Abu-Elaziz, and S. E. Ahmed, Int. Commun. Heat Mass Transfer **37**, 1504 (2010). https://doi.org/10.1016/j.icheatmasstransfer.2010.09.004
8. S. E. Ahmed, M. A. Mansour, A. K. Hussein, and S. Sivasankaran, Eng. Sci. Technol. Int. J. **19**, 364 (2016).
9. S. Parvin and R. Nasrin, Nonlinear Analysis: Modelling Control **16**, 89 (2011). https://doi.org/10.15388/NA.16.1.14117
10. M. M. Billah, M. M. Rahman, M. Shahabuddin, and A. K. Azad, J. Sci. Res. **3**, 525 (2011). https://doi.org/10.3329/jsr.v3i3.7642

11. E. Abu-Nada and H. F. Oztop, Int. J. Heat Fluid Flow **30**, 669 (2009). https://doi.org/10.1016/j.ijheatfluidflow.2009.02.001
12. H. F. Oztop and E. Abu-Nada, Int. J. Heat Fluid Flow **29**, 1326 (2008). https://doi.org/10.1016/j.ijheatfluidflow.2008.04.009
13. F.-Z. Bensouici and S. Boudebous, Fluid Dynamics Mater. Process. **13**, 189 (2017).
14. G. Guo and M. A. R. Sharif, Int. J. Thermal Sci. **43**, 465 (2004). https://doi.org/10.1016/j.ijthermalsci.2003.08.008
15. H. C. Brinkman, J. Chem. Phys. **20**, 571 (1952). https://doi.org/10.1063/1.1700493
16. J. C. M. Garnett, Math. Phys. Eng. Sci**.** **203**, 385 (1904). https://doi.org/10.1098/rsta.1904.0024
17. S. Parvin and R. Nasrin, J. Sci. Res. **4**, 337 (2012). https://doi.org/10.3329/jsr.v4i2.8142
18. M. J. H. Munshi and M. A. Alim, J. Sci. Res. **9**, 1 (2016). https://doi.org/10.3329/jsr.v1i1.27702
19. M. J. H. Munshi, M. A. Alim, M. Ali, and M. S. Alam, J. Sci. Res. **9**, 145 (2017). https://doi.org/10.3329/jsr.v9i2.29644
20. C. S. Balla, N. K. Rama S. R. Gorla, and B. J. Gireesha, Ain Shams Eng. J. **8**, 237 (2017). https://doi.org/10.1016/j.asej.2016.02.010
21. A. M. Rashad, S. E. Ahmed, Khan, A. Waqar, and M. A. Mansour, J. Nanofluids **6**, 368 (2017). https://doi.org/10.1166/jon.2017.1324
22. A. M. Aly, E. M. Mohamed, and N. Alsedais, Case Studies in Thermal Eng. **25**, ID 100945 (2021). https://doi.org/10.1016/j.csite.2021.100945
23. S. Saleem, A. Shafee, M. Nawaz, R. N. Dara, I. Tlili, and E. Bonyah, AIP Adv. **9**, ID 095107 (2019). https://doi.org/10.1063/1.5120439
24. C. Sulochana and T. P. Kumar, Heat Transfer, **51**, 4485 (2022). https://doi.org/10.1002/htj.22509
25. C. Sulochana and T. P. Kumar, Materialstoday Proc. **54**, 669 (2022). https://doi.org/10.1016/j.matpr.2021.10.375
26. A. Akter and S. Parvin, J. Sci. Res. **10**, 11 (2018). https://doi.org/10.3329/jsr.v10i1.33848